Applied Physics Letters

RESEARCH ARTICLE | MAY 28 2024

Epitaxially regrown quantum dot photonic crystal surface emitting lasers

Aye S. M. Kyaw ; Ben C. King ; Adam F. McKenzie ; Zijun Bian ; Daehyun Kim; Neil D. Gerrard; Kenichi Nishi ; Keizo Takemasa; Mitsuru Sugawara; David T. D. Childs; Calum H. Hill ; Richard J. E. Taylor ; Richard A. Hogg

Appl. Phys. Lett. 124, 221101 (2024)
https://doi.org/10.1063/5.0202834

06 June 2024 13:10:08

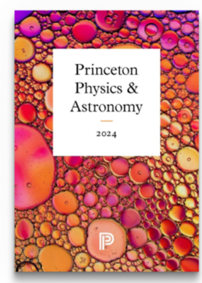

Browse our new Physics and Astronomy Catalog
30% off titles with code **P326**

Applied Physics Letters ARTICLE pubs.aip.org/aip/apl

Epitaxially regrown quantum dot photonic crystal surface emitting lasers

Cite as: Appl. Phys. Lett. **124**, 221101 (2024); doi: 10.1063/5.0202834
Submitted: 7 February 2024 · Accepted: 11 May 2024 ·
Published Online: 28 May 2024

Aye S. M. Kyaw,[1,a)] Ben C. King,[1] Adam F. McKenzie,[1] Zijun Bian,[1] Daehyun Kim,[1] Neil D. Gerrard,[2] Kenichi Nishi,[3] Keizo Takemasa,[3] Mitsuru Sugawara,[3] David T. D. Childs,[4] Calum H. Hill,[4] Richard J. E. Taylor,[4] and Richard A. Hogg[1,5]

AFFILIATIONS

[1]James Watt School of Engineering, University of Glasgow, Glasgow G12 8QQ, United Kingdom
[2]III-V Epi Ltd., 11 The Square, University Avenue, Glasgow G12 8QQ, United Kingdom
[3]QD Laser Inc., Minamiwataridacho, Kawaski-ku, Kawasaki, Kanagawa 210-0855, Japan
[4]Vector Photonics Ltd., 2317 Maryhill Rd., Glasgow G20 0SP, United Kingdom
[5]Aston Institute of Photonic Technologies, Aston University, Birmingham B4 7ET, United Kingdom

[a)]Author to whom correspondence should be addressed: ayesumon.kyaw@glasgow.ac.uk

ABSTRACT

Quantum dot-based epitaxially regrown photonic crystal surface emitting lasers are demonstrated at room temperature. The GaAs-based devices, which are monolithically integrated on the same wafer, exhibit ground state lasing at ∼1230 nm and excited state lasing at ∼1140 nm with threshold current densities of 0.69 and 1.05 kA/cm^2, respectively.

© 2024 Author(s). All article content, except where otherwise noted, is licensed under a Creative Commons Attribution (CC BY) license (https://creativecommons.org/licenses/by/4.0/). https://doi.org/10.1063/5.0202834

06 June 2024 13:10:08

Photonic crystal surface emitting lasers (PCSELs) have emerged as a new class of semiconductor lasers that incorporate a two-dimensional (2D) photonic crystal (PC) within the device structure. They have drawn significant attention due to the possibility for simultaneous high-power and single-mode vertical emission with narrow divergence, beam steering,[1] and control of the wavelength, and polarization.[2] The first PCSELs were demonstrated in 1999 using an organic gain medium[3] and in InP.[4] Since then, research into PCSELs has advanced rapidly in a number of different material systems, such as GaN,[5,6] GaAs,[7–9] InP,[10,11] and GaSb,[12,13] with wavelengths spanning the visible to THz regions.[14]

While techniques such as wafer fusion[4] and the use of deeply etched surface gratings[15] have been utilized previously, epitaxial regrowth has become the preferred method for fabricating PCSELs owing to the elimination of detrimental defects associated with other techniques.[16,17] Epitaxial regrowth also offers greater flexibility in PC design, allowing for both void/semiconductor contrast PCSELs[18] and all-semiconductor PCSELs[16,17] to be realized. Epitaxial regrowth has been highlighted as a key enabler in the realization of high power and high efficiency of PCSEL.[19] To date, void-containing PCSELs have demonstrated the best performance in terms of power and efficiency due to the large refractive index difference between the void (n ∼ 1) and semiconductor (n ∼ 3) and the large associated coupling coefficients of the PC layer.[18]

As the gain medium in PCSELs, quantum wells (QWs) have so far been near-universally used. The integration of a quantum dot (QD) active media, however, would provide a number of significant advantages. They offer extended wavelength operation as compared to QWs (e.g., 1.3 μm lasers on GaAs substrates), temperature-insensitive operation,[20] low threshold current density,[21] and feedback insensitivity, which is especially of interest for silicon photonics.[22] Additionally, the ability to utilize both the ground state (GS) and excited state (ES) of the QDs would allow for multiple emission wavelengths from one heterostructure, with the ES offering both higher saturated gain and direct modulation rates.[23] Previously, optically and electrically pumped QD-based PCSELs have been demonstrated utilizing deep etching and the use of transparent contact layers.[24,25]

Here, we describe epitaxially regrown QD-based PCSELs. Our approach utilizes well-established molecular beam epitaxy (MBE) processes for the QD epitaxy and recently developed void-retaining epitaxy via metalorganic vapor-phase epitaxy (MOVPE). We show that the choice of the PC grating period can be tuned to allow for emission at either the GS or ES of the QDs, 90 nm apart in wavelength,

© Author(s) 2024

monolithically on the same wafer. Following this, we explore the effect of various PC design parameters on device characteristics.

Figure 1 shows a schematic of the complete QD-PCSEL device structure. The base epitaxy material was grown on a n-GaAs (100) substrate by MBE under almost identical conditions to those detailed in a previous report.[26] The structure consists of a 300 nm n-GaAs buffer layer followed by 20 nm n-$Al_{0.2}Ga_{0.8}As$, 1440 nm n-$Al_{0.4}Ga_{0.8}As$, and 20 nm n-$Al_{0.2}Ga_{0.8}As$, which act as cladding layers. This is followed by eight layers of QDs and 388 nm of p-GaAs. The growth of the active region starts with 60 nm of undoped GaAs followed by eight layers of InAs QDs. The thickness of the InAs layer is 0.8 nm and 39.2 nm-thick undoped-GaAs barriers are inserted between the layers of QDs to allow stacking of multiple layers. The emission of the GS and ES of the QDs is centered at $\sim$1230 and $\sim$1140 nm, respectively. The period, a, of the second-order PC grating is $\frac{\lambda}{n_{eff}}$ where λ is the lasing wavelength and n_{eff} is the effective refractive index of the layer. Careful design of the lattice period to align with the GS and ES peaks of the QDs will allow the monolithic integration of two different wavelength devices on a single wafer. In addition to the grating period, engineering of the PC design in the vertical (out-of-plane) and horizontal (in-plane) directions (e.g., pit etch depth and PC atom shape, respectively) is also important to enhance the lasing performance.

To fabricate the PC gratings, 200 nm of SiO_2 was deposited on the surface of the upper p-GaAs layer by plasma-enhanced chemical vapor deposition (PECVD). The PC patterns were defined by electron-beam lithography in PMMA and etched into the SiO_2 by reactive ion etching (RIE) with CHF_3/Ar chemistry. This SiO_2 acts as a hard mask for the subsequent etching of the underlying semiconductor. The PC is then transferred into the top p-GaAs layer of base wafer by inductively coupled plasma (ICP) etching with a $BlC_3/Cl_2/Ar/N_2$ chemistry. The SiO_2 is then removed and the wafer surface cleaned by a combined HF and UV/ozone treatment prior to epitaxial regrowth. The upper cladding layers were deposited by MOVPE at 650 °C. The regrowth structure consists of 400 nm of low-doped p-$Al_{0.35}GaAs$ infill layer, which encapsulates the PC layer, followed by 1500 nm of higher-doped p-$Al_{0.37}GaAs$ layer, and a 100 nm-thick p^+-GaAs contact layer. Details of the growth conditions used for grating infill, as well as analysis of void formation in this and similar structures, have been recently reported elsewhere.[27]

Following regrowth, a square mesa is etched to a depth of 1 μm using a combination of photolithography and dry etching to electrically isolate the devices. The mesa widths range from 200 to 800 μm. This mesa depth was chosen to maximize the isolation but not present a reflective facet to the in-plane optical mode. A 200 nm-thick SiO_2 passivation layer was then deposited across the wafer and a contact window opened with CHF_3 and Ar-based RIE, after which a p-type Ti/Pt/Au contact was deposited. Finally, an n-type Ni/Au/Ge/Ni/Au contact layer was deposited on the back of the wafer, and an emission aperture was defined in this contact using a combination of standard photolithography-based liftoff process, after which the sample was annealed at 400 °C for 1 min. Fabrication was then completed by the deposition of a thick Ti/Au bond pad on the top surface. A schematic of the complete substrate-emitting device is shown in Fig. 2.

The lasing characteristics of the devices were measured at room temperature under quasi-CW conditions with a duty cycle of 1% and pulse width of 10 μs. The reported output power of the devices is expected to be underestimated by a factor of three due to absorption in the un-thinned substrate and reflection at the semiconductor/air interface. In the future, these losses may be minimized by thinning of the substrate material prior to deposition of the n-type contact and the introduction of anti-reflection coatings.

Initially, the realization of monolithic two-color QD-PCSEL devices by engineering the PC lattice periods is discussed. Two lattice periods of 341 and 370 nm were chosen, targeting the ES and GS of QD, respectively. In each case, the PC region is $400 \times 400\ \mu m^2$ in area and consisted of a square lattice of circular air holes with radius, r, chosen to give an r/a value of 0.2. Plan-view SEM images of both gratings before regrowth are shown in Figs. 3(a) and 3(b). Figures 3(c) and 3(d) plot the simulated band structure of the QD-PCSEL. This was obtained using structural data of the devices, via 1D waveguide simulation of the PC atom and field, and plane wave expansion.

FIG. 1. Schematic structure of the QD-PCSEL. The base epitaxy material, which includes eight layers of InAs QDs, was grown by MBE. The upper cladding layers, which encapsulate the PC layer, were regrown by MOVPE.

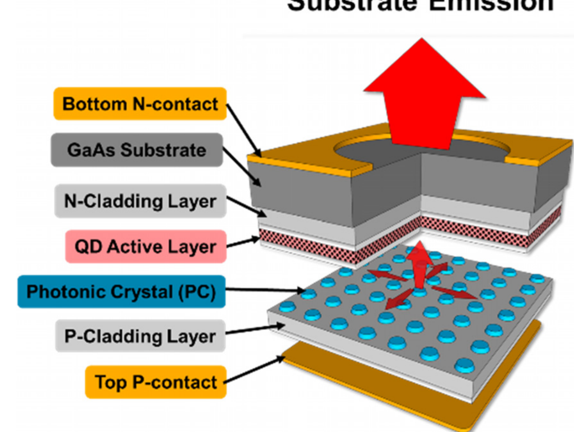

FIG. 2. Schematic illustration of substrate-emitting QD-PCSEL structure. Lasing is enabled by a square lattice PC defined in the p-type layers of the device. Emission is through a circular aperture opened in the n-metal contact.

06 June 2024 13:10:08

© Author(s) 2024

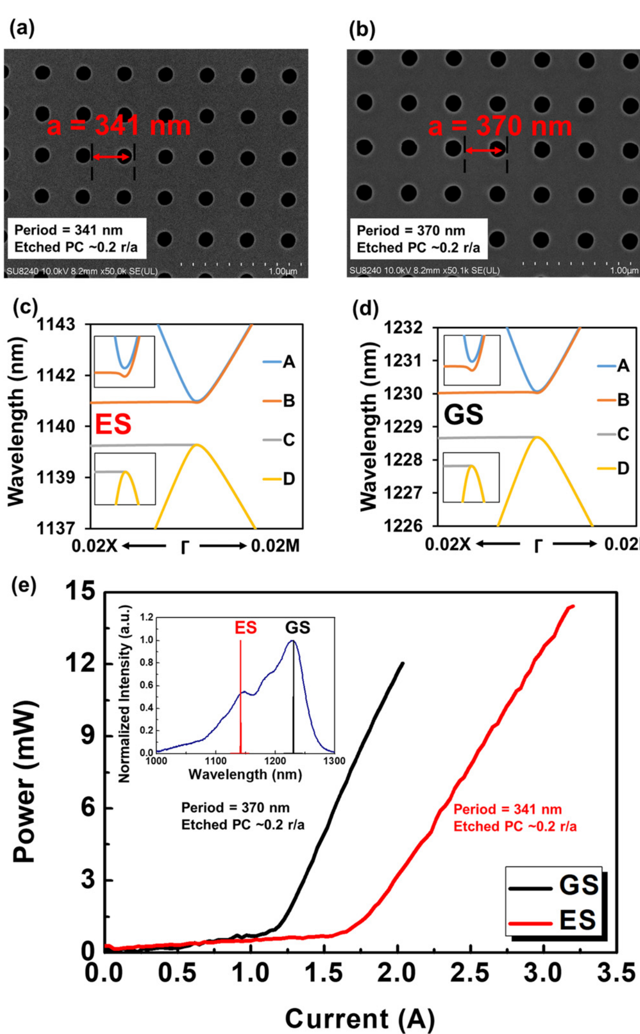

FIG. 3. Plan-view SEM images of PC gratings with period, a, of (a) 341 and (b) 370 nm, corresponding to GS and ES lasing, respectively. The radii, r, of the circular pits are such that their r/a values are 0.2. The simulated band structure of a square lattice, circular PC with period, a, of (c) 341 and (d) 370 nm. (e) LI characteristics of the GS (black) and ES (red) devices. The corresponding emission peaks at ∼1230 and ∼1141 nm are shown, inset, together with the spontaneous emission spectrum of the QDs (blue).

The corresponding LI curves are shown in Fig. 3(e), demonstrating both GS (black) and ES (red) lasing. GS lasing is obtained at a threshold current of 1.1 A (J = 0.69 kA/cm^2) with a slope efficiency of 13.4 mW/A. The threshold current for ES lasing is 1.6 A (J = 1.05 kA/cm^2) with a slope efficiency of 9.5 mW/A. The threshold current of ES lasing is higher than that of GS because of the higher degeneracy of the ES and the need to saturate GS gain to achieve ES lasing. Conformation of PC pitch selective lasing from the GS or ES is given in the inset of Fig. 3(c), which shows the sub-threshold electroluminescence spectrum (blue) of the QD material (as measure at 0.5 A) together with the normalized GS and ES lasing peaks at wavelengths of ∼1230 and ∼1141 nm, respectively. The lasing linewidth is measured to be 0.3 nm, limited by the resolution of the measurement apparatus.

We estimate the threshold modal gain to be ∼25 cm^{-1}, allowing an estimate of the losses within the cavity. The radiative loss is ∼0.4 cm^{-1}, and total parasitic loss (in-plane and internal loss) is ∼24.4 cm^{-1}.

The effect of PC etch depth on the lasing characteristics of ES devices is next discussed. Two etch depths of 300 and 400 nm are considered. In this case, the PC region is 600 × 600 μm^2 in area and consists of a square lattice of circular air holes with a larger r/a value of 0.4. Cross-sectional scanning transmission electron microscopy (STEM) images of the PCs after regrowth, shown in Figs. 4(a) and 4(b), indicate that a significant difference in void height on the order of 80 nm is obtained, owing to the difference in grating etch depths.

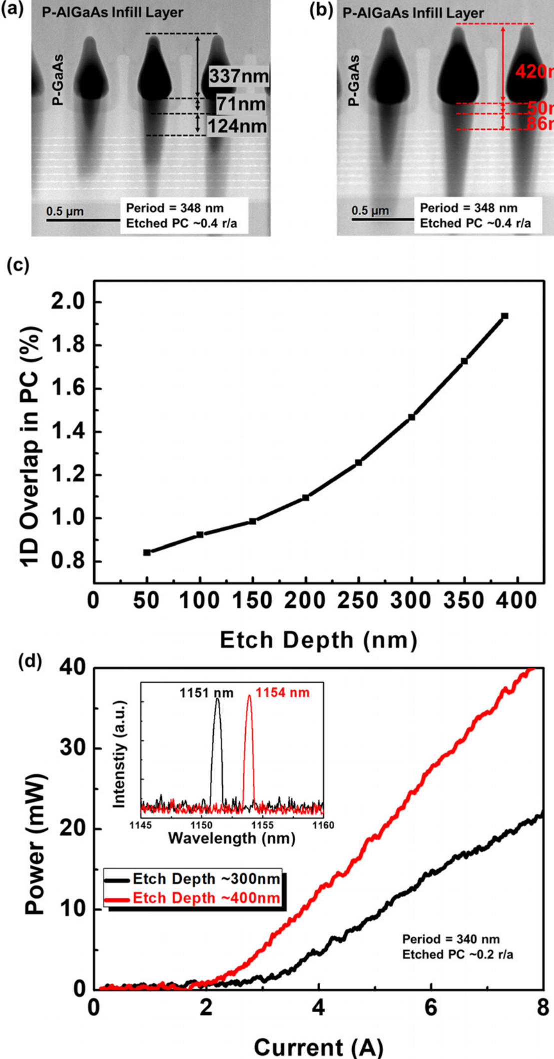

FIG. 4. Cross-sectional STEM images of voids formed after regrowth of PC pits with etch depths of (a) 300 and (b) 400 nm. The r/a value for both pits is 0.4. (c) Simulated 1D overlap in PC as a function of etch depth. (d) LI characteristics of corresponding PCSEL devices. The reduction in threshold current for the deeper etched device is the result of enhanced mode overlap and in-plane coupling. ES lasing spectra are shown in the inset.

06 June 2024 13:10:08

© Author(s) 2024

The corresponding LI curves for the devices are shown in Fig. 4(c). In the case of the shallower etch depth device, a threshold current of 3 A ($J = 0.83\,kA/cm^2$) and slope efficiency of 4.4 mW/A are obtained. The deeper etched device, however, displays improved performance, having a reduced threshold current of 2.1 A ($J = 0.58\,kA/cm^2$) and increased slope efficiency of 7.5 mW/A. This improvement can be explained by considering the void geometry in each case. In order to achieve high output powers from PCSELs, the PC layer must be close to the active region, maximizing mode overlap between the two,[28] and the layer thickness (in this case, void height) must be optimized to minimize destructive interference of the vertically scattered light.[29] In addition to the increased void height described above, the PC in the deeper etched device displays a reduced separation of approximately 136 nm (compared with 195 nm for the shallower etch device), thereby increasing mode overlap with the PC layer, leading to stronger in-plane coupling, reduced threshold current, and higher slope efficiency. The inset of Fig. 4(c) shows the lasing spectra of both devices. The lasing wavelengths are ~1151 and ~1154 nm for etch depths of 400 and 300 nm, respectively. As the etch depth increases, the effective refractive index decreases, and therefore the lasing wavelength is shifted to a shorter wavelength.

Next, the effect of in-plane PC engineering on the characteristics of ES lasing is explored though variation in atom shape. In this case, the PC is a square lattice with an area of $200 \times 200\,\mu m^2$, and two atom shapes are considered; circular air holes with r/a value of 0.2 and a triangular air hole with *l*/a value of 0.5, where *l* is the length of the right-angled edge. Plan-view SEM images of the PC layers prior to regrowth are shown in Figs. 5(a) and 5(b). The corresponding LI curves for the devices are shown in Fig. 5(c). The device containing circular atoms exhibits a threshold current of 0.5 A ($J = 1.25\,kA/cm^2$) and a slope efficiency of 4.1 mW/A. By contrast, the device containing triangular atoms exhibits a significantly higher threshold current of 1.8 A ($J = 4.5\,kA/cm^2$), which is attributed to increased losses associated with an unoptimized PC etch process for triangular pits (reduced etch depth as compared to the circular pattern that has a higher fill-factor). However, the slope efficiency of the device is broadly comparable to that of the circular atoms at 4.2 mW/A, which, accounting for increased internal losses, attests to the higher out-of-plane coupling strength associated with reduced in-plane symmetry of the triangular PC atom.[30,31] We note that triangular atoms have provided significant improvements in PCSEL operation[18] and that this result should be placed in context with those results. The lasing spectra for the devices are shown in the inset of Fig. 5(c). The lasing wavelengths of the circular and triangular atoms are ~1153 and ~1152 nm. Here, the slight blue shifting of emission wavelength is attributed to slightly larger voids forming within triangular pits.

Finally, the effect of varying PC area is discussed. Here, the PCs consist of a square lattice of circular atoms with an r/a value of 0.2, covering areas of $200 \times 200\,\mu m^2$, $400 \times 400\,\mu m^2$, and $600 \times 600\,\mu m^2$. The corresponding LI characteristics, which are plotted in Fig. 6, show a significant decrease in threshold current density with increasing PC area. For the smallest device, the large current density ($J = 1.5\,kA/cm^2$) is attributed to high in-plane losses from the edges of the PC. These parasitic losses are less significant as the PCSEL area is scaled, leading to a reduction in threshold current density. It should be noted that thermal effects may also contribute to an effective increase in threshold current density and reduction in slope efficiency as area is scaled.

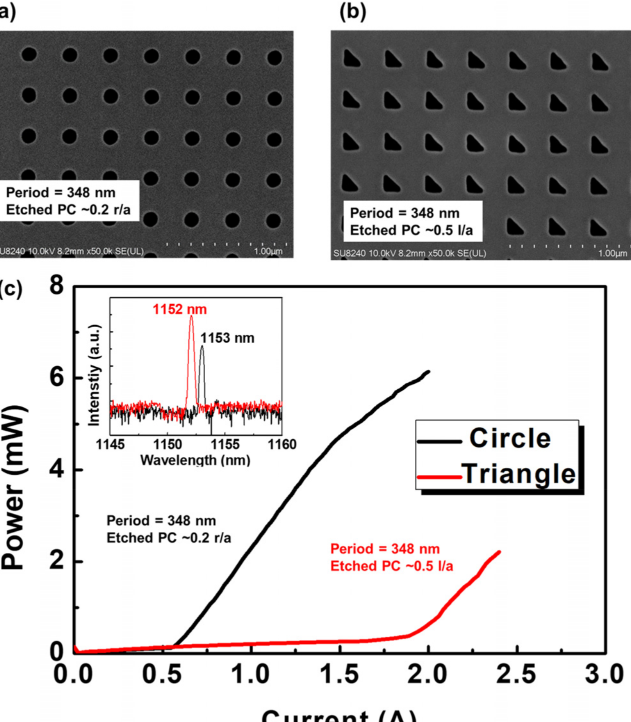

FIG. 5. Plan-view SEM images of PC gratings with different atom shapes: (a) 0.2 r/a circles and (b) 0.5 l/a triangles. (c) Corresponding LI characteristics showing a large reduction in threshold current for device using circular atoms. ES lasing spectra are shown in the inset.

While low threshold current densities are a key attraction for the use of QD actives, we note that the threshold current densities here are comparable to those of conventional quantum well active PCSELs. Current PCSEL designs have high threshold gains that require multilayer stacks of high areal density QDs to support lasing. As designs

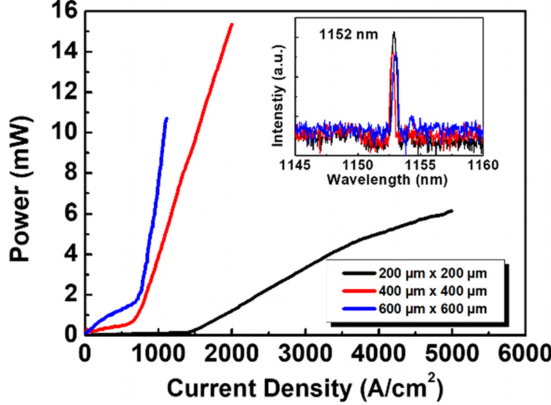

FIG. 6. LJ characteristics of PCSEL containing PC gratings with different total areas. The PC consists of circular atoms with r/a values of 0.2. The significant reduction in threshold current density for larger devices is due to reduced in-plane and scattering losses. ES lasing spectra are shown in the inset.

06 June 2024 13:10:08

© Author(s) 2024

and fabrication technologies reduce parasitic losses, we can expect QD-based structures to deliver on low threshold current density devices.

We have reported the demonstration of QD-based epitaxially regrown PCSELs. For GaAs-based devices utilizing InAs QDs, it has been shown that both GS and ES lasers can be realized monolithically on a single wafer by the tuning of PC grating period. GS lasing at ∼1230 nm and ES lasing at ∼1140 nm were achieved with threshold current densities of 0.69 and 1.05 kA/cm^2, respectively, at room temperature. Beyond this, the dependence of ES lasing characteristics (threshold current density and slope efficiency) on various PC design aspects, including void size, atom shape, and total PC area, have been discussed.

This work was supported by Innovate UK/Eurostars Project “BLOODLINE” (Grant No. 79455). B.C.K. is grateful for the support provided by the Engineering and Physical Sciences Research Council (RCUK Grant No. EP/L015323/1). A.F.M. is grateful for the support of the Royal Commission for the Exhibition of 1851 through an Industrial Fellowship (Grant No. IF195/2018).

AUTHOR DECLARATIONS

Conflict of Interest

The authors have no conflicts to disclose.

Author Contributions

Aye S. M. Kyaw: Data curation (lead); Formal analysis (lead); Investigation (lead); Methodology (lead); Visualization (lead); Writing – original draft (lead); Writing – review & editing (lead). **Ben C. King:** Methodology (equal). **Adam F. McKenzie:** Investigation (equal); Methodology (equal). **Zijun Bian:** Methodology (equal). **Daehyun Kim:** Methodology (equal). **Neil D. Gerrard:** Methodology (equal); Resources (equal). **Kenishi Nishi:** Methodology (equal); Resources (equal). **Keizo Takemasa:** Resources (equal). **Mitsuru Sugawara:** Resources (equal); Supervision (equal). **David T. D. Childs:** Funding acquisition (equal); Methodology (equal); Supervision (equal). **Calum H. Hill:** Methodology (equal). **Richard J. E. Taylor:** Funding acquisition (equal). **Richard A. Hogg:** Conceptualization (equal); Funding acquisition (equal); Supervision (equal); Writing – original draft (equal); Writing – review & editing (equal).

DATA AVAILABILITY

The data that support the findings of this study are available from the corresponding author upon reasonable request.

REFERENCES

[1] Y. Kurosaka, S. Iwahashi, Y. Liang, K. Sakai, E. Miyai, W. Kunishi, D. Ohnishi, and S. Noda, Nat. Photonics **4**(7), 447–450 (2010).
[2] M. Imada, A. Chutinan, S. Noda, and M. Mochizuki, Phys. Rev. B **65**(19), 1953086 (2006).
[3] M. Meier, A. Mekis, A. Dodabalapur, A. Timko, R. E. Slusher, J. D. Joannopoulos, and O. Nlamasu, Appl. Phys. Lett. **74**(1), 7–9 (1999).
[4] M. Imada, S. Noda, A. Chutinan, M. Murata, and G. Sasaki, IEEE J. Sel. Top. Quantum Electron. **5**(3), 658–662 (1999).
[5] H. Matsubara, S. Yoshimoto, H. Saito, Y. Jianglin, Y. Tanaka, and S. Noda, Science **319**, 445–447 (2008).
[6] T. C. Lu, S. W. Chen, L. F. Lin, T. T. Kao, C. C. Kao, P. Yu, H. C. Kuo, S. C. Wang, and S. Fan, Appl. Phys. Lett. **93**, 111111 (2008).
[7] M. Yoshida, M. D. Zoysa, K. Ishizaki, Y. Tanaka, M. Kawasaki, R. Hatsuda, B. Song, J. Gelleta, and S. Noda, Nat. Mater. **18**, 121–128 (2019).
[8] B. C. King, K. J. Rae, A. F. McKenzie, A. Boldin, D. Kim, N. D. Gerrard, G. Li, K. Nishi, K. Takemasa, M. Sugawara, R. J. Taylor, D. T. D. Childs, and R. A. Hogg, AIP Adv. **11**, 015017 (2021).
[9] K.-B. Hong, L.-R. Chen, K.-C. Huang, H.-T. Yen, W.-C. Weng, B.-H. Chuang, and T.-C. Lu, IEEE J. Sel. Top. Quantum Electron. **28**(1), 1700207 (2022).
[10] Z. Bian, K. J. Rae, A. F. McKenzie, B. C. King, N. Babazadeh, G. Li, J. R. Orchard, N. D. Gerrard, S. Thomas, D. A. MacLaren, R. J. E. Taylor, D. Childs, and R. A. Hogg, IEEE Photonics Technol. Lett. **32**(24), 1531–1534 (2020).
[11] Y. Itoh, N. Kono, D. Inoue, N. Fujiwara, M. Ogasawara, K. Fujii, H. Yoshinaga, H. Yagi, M. Yoshida, T. Inoue, M. D. Zoysa, K. Ishizaki, and S. Noda, Opt. Express **30**(16), 29539 (2022).
[12] R. Liu, L. Shterengas, A. Stein, G. Kipshidze, D. Zakharov, K. Kisslinger, and G. L. Belenky, Photonics **9**, 891 (2022).
[13] Y.-H. Huang, Z.-X. Yang, S.-L. Cheng, C.-H. Lin, G. Lin, K.-W. Sun, and C.-P. Lee, Micromachines **12**, 468 (2021).
[14] Z. Wang, Y. Liang, B. Meng, Y.-T. Sun, G. Omanakuttan, E. Gini, M. Beck, I. Sergachev, S. Lourdudoss, J. Faist, and G. Scalari, Opt. Express **27**(16), 22708 (2019).
[15] M.-Y. Hsu, G. Lin, and C.-H. Pan, Opt. Express **25**(26), 32697–32704 (2017).
[16] D. M. Williams, K. M. Groom, B. J. Stevens, D. T. D. Childs, R. J. E. Taylor, S. Khamas, R. A. Hogg, N. Ikeda, and Y. Sugimoto, IEEE Photonics Technol. Lett. **24**(11), 966–968 (2012).
[17] R. J. E. Talyor, D. M. Williams, D. T. D. Childs, B. J. Stevens, L. R. Shepherd, S. Khamas, K. M. Groom, R. A. Hogg, N. Ikeda, and Y. Sugimoto, IEEE J. Sel. Top. Quantum Electron. **19**(4), 4900407 (2013).
[18] K. Hirose, Y. Liang, Y. Kurosaka, A. Watanbe, T. Sugiyama, and S. Noda, Nat. Photonics **8**(5), 406–411 (2014).
[19] K. Ishizaki, M. D. Zoysa, and S. Noda, Photonics **6**(3), 96 (2019).
[20] S. Fathpour, Z. Mi, P. Bhattacharya, A. R. Kovsh, S. S. Mikhrin, I. L. Krestnikov, A. V. Kozhukhov, and N. N. Ledentsov, Appl. Phys. Lett. **85**(22), 5174–5166 (2004).
[21] H. Y. Liu, D. T. Childs, T. J. Badcock, K. M. Groom, I. R. Sellers, M. Hopkinson, R. A. Hogg, D. J. Robbins, D. J. Mowbray, and M. S. Skolnick, IEEE Photonics Technol. Lett. **17**(6), 1139–1141 (2005).
[22] C. Shang, Y. Wan, J. Selvidge, E. Hughes, R. Herrick, K. Mukherjee, J. Duan, F. Grillot, W. W. Chow, and J. E. Bowers, ACS Photonics **8**(9), 2555–2566 (2021).
[23] B. J. Stephens, D. T. D. Childs, H. Shahid, and R. A. Hogg, Appl. Phys. Lett. **95**(6), 061101 (2009).
[24] T.-S. Chen, Z.-L. Li, M.-Y. Hsu, G. Lin, and S.-D. Lin, J. Lightwave Technol. **35**(20), 4547–4552 (2017).
[25] H.-Y. Lu, S.-C. Tian, C.-Z. Tong, L.-J. Wang, J.-M. Rong, C.-Y. Liu, H. Wang, S.-L. Shu, and L.-J. Wang, Light **8**(1), 108 (2019).
[26] A. F. McKenzie, A. M. Kyaw, N. D. Gerrard, D. A. MacLaren, and R. A. Hogg, J. Cryst. Growth **602**, 126969 (2023).
[27] K. Nishi, T. Kageyama, M. Yamaguchi, Y. Maeda, K. Takemasa, T. Yamomoto, M. Sugawara, and Y. Arakawa, J. Cryst. Growth **378**, 459–462 (2013).
[28] R. J. E. Taylor, D. M. Williams, J. R. Orchard, D. T. D. Childs, S. Khamas, and R. A. Hogg, Phys. D **46**, 264005 (2013).
[29] S. Iwahashi, K. Sakai, Y. Kurosaka, and S. Noda, J. Opt. Soc. Am. B **27**(6), 1204–1207 (2010).
[30] Y. Kurosaka, K. Sakai, E. Miyai, and S. Noda, Opt. Express **16**(22), 18485 (2008).
[31] C. Peng, Y. Liang, K. Sakai, S. Iwahashi, and S. Noda, Opt. Express **19**(24), 24672 (2011).

06 June 2024 13:10:08

© Author(s) 2024